Available online at www.sciencedirect.com
ScienceDirect
Journal of Sound and Vibration 308 (2007) 721–734
JOURNAL OF SOUND AND VIBRATION
www.elsevier.com/locate/jsvi

Effect of surface topography on mode-coupling model of dry contact sliding systems

Meifal Rusli*, Masaaki Okuma

Department of Mechanical and Aerospace Engineering, Tokyo Institute of Technology, 2-12-1-I3-15, O-okayama, Meguro-ku, Tokyo 152-8552, Japan

Accepted 22 March 2007
The peer review of this article was organised by the Guest Editor
Available online 13 June 2007

Abstract

Dry contact sliding between two structures is frequently found to generate squeal noise in certain topography condition of contact surface. Furthermore, a different surface topography may generate squeal noise at different frequencies. In this paper, authors investigate the effect of topography of contact surfaces to the normal contact stiffness, the tangential contact stiffness, and the friction coefficient. The normal and tangential contact stiffness are determined by a classical model of asperity on contact surface. These parameters will be the dominant factors of the squeal noise generation by means of mode-coupling analysis. Numerical simulation-based investigation is carried out using two simple models, i.e. a two-degree of freedom model and a simple space frame model. The simulation results show that a structure has only one or few pairs of couple modes with complex eigenvalues at certain contact conditions. For a system with multi-degrees of freedom, some mode shapes make couples in different contact conditions. On the other hand, smoother contact surfaces have higher normal and tangential contact stiffness. Furthermore, higher tangential contact stiffness and higher coefficient of friction will increase the possibility of squeal generation. Hence, it is understandable why the squeal noise appears and vanishes in some surface topography and has different frequencies at different values of surface roughness.

1. Introduction

Squeal noise is found to originate from the unstable vibratory response due to friction-induced vibration corresponding to only one or few natural frequencies of a structure. Two typical mechanical systems that frequently generate squeal noise are train-wheels on a curved track [1–5] and brake systems [6–11].

There are several kinds of mechanisms that cause squeal noise. Ibrahim reviewed many theorems and mechanisms in the literature [12]. Four typical mechanisms are stick–slip, sprag–slip, negative friction velocity slope, and mode coupling of structures. It was proved theoretically that stick–slip mechanism, sprag–slip, and negative friction velocity slope can cause chaos and instability of the systems, but these theoretical models cannot explain all events related to the squeal noise.

*Corresponding author. Tel./fax: +81 3 5734 3827.
E-mail address: meifal@stu.mech.titech.ac.jp (M. Rusli).

0022-460X/$ - see front matter © 2007 Elsevier Ltd. All rights reserved.
doi:10.1016/j.jsv.2007.03.046

Nomenclature

A_a	apparent contact area	$\beta_{1,2}$	mean radius of asperities of surface 1 and 2
d	distance between two surfaces	δ	deflection
D	nondimensional separation	φ	misalignment factor of two asperities in normal direction
E'	composite modulus elasticity	ξ	misalignment factor of two asperities in tangential direction
$E_{1,2}$	modulus elasticity of contact material 1 and 2	ξ/φ	correction factor of tangential contact stiffness
F_f	friction force	η	density of Asperities per unit area
F_n	normal force	$\eta_{1,2}$	density of asperities per unit area surface 1 and 2
k_n	normal contact stiffness		
k_t	tangential contact stiffness	μ	friction coefficient
p_a	apparent contact pressure	$v_{1,2}$	Poisson's ratio of contact material 1 and 2
s	normalized coordinate		
S_m	mean spacing between peaks	σ	standard deviation of height distribution asperities
R_p	maximum head profile		
W	normal load	$\sigma_{1,2}$	standard deviation of height distribution asperities surface 1 and 2
β	mean radius of asperities		

Furthermore, Chen et al. [13] reported that stick–slip occurs at slow relative sliding speed, but it does not appear at high relative sliding speed. In addition, when relative sliding speed becomes high enough and friction coefficient becomes a large value, the system emits squeal noise with very high sound pressure. Chen et al. [14] also found that there is no variable correlation between negative friction–velocity slope and the occurrence of squeal noise in reciprocating sliding systems. Squeal noise can occur in regions with both negative and positive friction–velocity slopes. In spite of all of this, mode coupling is generally acknowledged to be one of the most important mechanisms leading to self-excited vibration in relative sliding systems with friction [15].

Regarding the contact surface topography, by means of experimental analysis some researchers found that the roughness of relative sliding contact surfaces definitely influences the generation of the squeal noise. Eriksson et al. [10] investigated the relationship between brake pad surface topography and the occurrence of squeal noise. They found that the contact pressure of a sliding surface and the size of its plateaus have great influence on generating squeal noise. Pads with many small contact plateaus tend to generate strong squeal noise than pads with relatively large plateaus.

In the case of squeal noise of wheel in curve track, Eadie et al. [16] found that squeal noise could be avoided by change of the friction characteristics using a ''third body'' and the modification of contact surface between wheel and rail.

Furthermore, Chen et al. [17] investigated the correlation between squeal noise and topography characteristics of scars in reciprocating sliding. They observed that squeal noise is generated or vanished under certain scars conditions during the reciprocating sliding of two contact surfaces. Chen et al. [13] then found that two different vibration modes radiate squeal noise in different coefficient of friction due to changing the roughness of sliding surface. Besides, Sherif [18] proposed the concept of squeal index to describe the establishing the squeal noise. This index is a function with respect to the mean radius and the standard deviation of the height distribution of asperities of sliding surface.

In fact, it still remains many questions about scientifically obscure mechanisms to generate squeal noise. One of the questions is why squeal noise is generated in certain topography conditions and vanished in other conditions. This is to say, why a structure generates the squeal noise in rough contact surface but why others generate in relative smoother surface. Another one is which mode shapes are responsible to generate squeal noise, and how the roughness of contact surface affects the occurrence of vibration with the mode shapes.

In this paper, the authors investigate the effect of topography of sliding contact surfaces to the normal contact stiffness, tangential contact stiffness, and friction coefficient in squeal noise generation. The aims of

this paper are to answer the question why and how squeal noise is generated or vanished in certain surface topography conditions, and to predict which resonant modes are prone to generate squeal noise. The authors try to build "a simple bridge" to connect the tribology aspect and structural instability in the condition of generating squeal noise. The authors develop a simple contact surface model by taking the effect of tangential contact stiffness to the mechanism of generating squeal noise into account instead of the autonomous model proposed by Hoffman [19].

This paper consists of five sections. Following this introduction, in Section 2, the authors will review some theoretical and experimental analysis of contact parameters related to surface topography. These parameters are then used in the case studies using two kinds of computational models, i.e. a two-degree of freedom model and a simple space frame model in Sections 3 and 4, respectively. The discussion is focussed on a few couple resonant modes that make unstable modes at certain values of contact stiffness and friction coefficient. Here, the contact stiffness and friction coefficient can be expressed as the functions with respect to topography parameters. Finally in Section 5, this paper is concluded.

2. Contact model of rough surface

When two bodies having macroscopically flat but microscopically rough surface come into contact, the contact occurs at multiple asperities with arbitrary shapes, sizes and heights on the surface of both bodies. The deformation of the contact parts of the asperities can be elastic and/or elastic–plastic. When two surfaces slide relatively to each other, the adhesion of the asperities and other complex mechanisms of surface interaction generate friction force. The size and the number of contacting asperities strongly affect the interface conditions.

A number of modern approaches have been devoted to establish precise and practical modelling of contact surfaces over last three decades. However, the modelling is still very difficult today. The fact that the surface conditions are usually random and ambiguous makes it difficult to develop a purely theoretical and precise model; therefore stochastic models must be used. A classic statistical model based on a combination of elastic and plastic contact on rough surfaces was proposed firstly by Greenwood and Williamson (G&W model) [20,21]. The model assumed the surface composed of many hemispherical tipped asperities with an identical radius of curvature and a Gaussian distributed height about a mean plane of the surface. This statistical model is very limited because of over-simplified assumptions about the geometry of asperities, the distribution of the heights, and the neglect of interaction between adjacent asperities. Four realistic variations of the geometry of asperity are shown in Fig. 1. Nevertheless, G&W model can express a tendency about the effect of the surface properties to the area of real contact [22].

2.1. Normal contact stiffness

Hertzian analysis expresses the contact force between a spherical asperity with radius β and a plane in terms of the radius and the deflection by Eq. (1)

$$W_i = \tfrac{4}{3}E'\beta^{0.5}\delta^{1.5}, \tag{1}$$

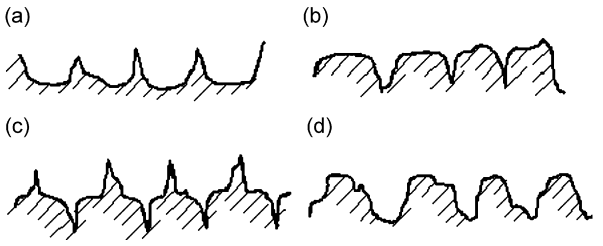

Fig. 1. Some variation of height and form of asperities [23]: (a) positive skewness; (b) negative skewness; (c) kurtosis higher than 3; and (d) kurtosis lower than 3.

where E' is a parameter of the composite modulus of elasticity related to Young's modulus and Poisson's ratios of a sphere and a plane of two body materials as expressed by

$$\frac{1}{E'} = \frac{1-v_1^2}{E_1} + \frac{1-v_2^2}{E_2}. \tag{2}$$

According to G&W model, it is considered that a plane is in contact with a nominally flat surface covered with a large number of spherically tipped asperities with same radius β and randomly distributed heights described by a probability density function $P(z)$. The model is depicted in Fig. 2. If the two surfaces come together until their reference planes are separated with the distance d, real contact occurs at any asperity whose height is originally greater than d. Thus, the probability of making contact at any given asperity of height z [21] is expressed by

$$P(z>d) = \int_d^\infty p(z)\,\mathrm{d}z. \tag{3}$$

If there are N asperities in all, the expected number of contacts is expressed as

$$n = N\int_d^\infty p(z)\,\mathrm{d}z. \tag{4}$$

Since $\delta = z - d$, the expected load W is expressed by

$$W = p_a A_a = \frac{4}{3}NE'\beta^{0.5}\int_d^\infty (z-d)^{1.5}p(z)\,\mathrm{d}z. \tag{5}$$

Since the number of asperities is defined by $N = \eta A$, and introducing a non-dimensional variable $D = d/\sigma$, the total load can be rewritten by Eq. (6).

$$W = \frac{4}{3}\eta A E'\beta^{0.5}\sigma^{1.5}\int_D^\infty (s-D)^{1.5}p^*(s)\,\mathrm{d}s, \tag{6}$$

where $p^*(s)$ is the standardized peak-height-probability density function, in which the distribution of the heights has been scaled to make its standard deviation be unity. For a Gaussian distribution the standardized peak-height-probability density function is expressed by

$$p^*(s) = \frac{1}{\sqrt{2\pi}}\exp\left(\frac{-s^2}{2}\right). \tag{7}$$

If two surfaces are mutually independent, the equivalent rough surface is defined as

$$\frac{1}{\beta} = \frac{1}{\beta_1} + \frac{1}{\beta_2}. \tag{8}$$

Using the assumption that all asperities are spherical, the mean radius of them on each contact surface is computed by Eq. (9) [18].

$$\beta_n = \frac{S_{mn}}{32R_{pn}} + \frac{R_{pn}}{2} \quad \text{for } n = 1, 2. \tag{9}$$

The standard deviation of the equivalent roughness of surface σ is expressed with the standard deviations of the two contact surfaces σ_1 and σ_2 as expressed by Eq. (10).

$$\sigma = (\sigma_1^2 + \sigma_2^2)^{1/2}. \tag{10}$$

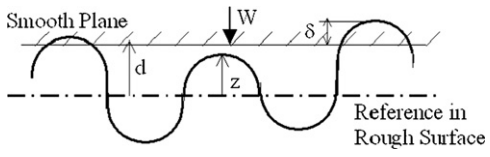

Fig. 2. Spherical tip of asperities contacted to a smooth plane.

The normal contact stiffness is defined by

$$k_n = \frac{\mathrm{d}W}{\mathrm{d}\delta}. \tag{11}$$

The chain-rule of differentiation changes Eq. (11) into Eq. (12).

$$k_n = \frac{\mathrm{d}W}{\mathrm{d}D}\frac{\mathrm{d}D}{\mathrm{d}\delta}. \tag{12}$$

Knowing that

$$D = \frac{d}{\sigma} = s - \frac{\delta}{\sigma}. \tag{13}$$

Eq. (12) can be rewritten as

$$k_n = 2\eta A E' \beta^{0.5}\sigma^{0.5}\int_D^{\infty}(s-D)^{0.5}p^*(s)\,\mathrm{d}s. \tag{14}$$

According to Bhushan [23], for a Gaussian distribution of the height of asperities, D is obtained by Eq. (15)

$$D = 1.4(\log(0.57/P_a))^{0.65}, \tag{15}$$

where

$$P_a = \frac{p_a}{(\eta\beta\sigma)E'\left(\frac{\sigma}{\beta}\right)^{1/2}} \leqslant 0.57. \tag{16}$$

When two surfaces are in contact, their encountered asperities touch elastically and/or plastically. During sliding, asperities deform elastically and/or plastically to ride over each other in contact condition. They are subjected to loading and unloading fatigue cycles, impacts that depend on the density of asperities of the surfaces and the relative speed of sliding.

2.2. Tangential contact stiffness

For the dynamic analyses of structural systems having friction contact in them, two types of modelling approaches are widely used for dealing with friction contact, i.e. the macro slip and the micro slip modelling approach. The macro slip modelling approach is usually applied to the analyses under the assumption that the friction interface is modelled as rigid surfaces and that interface is entirely in stick or slip states. On the other hand, the micro slip modelling approach accepts the elasticity of friction interface, so that it is capable for modelling partial slip.

In fact, it is thought that the contact interfaces in vibrating structures are subjected to oscillatory relative motion. Then, the characteristics are essentially theorized base on their hysteresis cycles that can show how the tangential force varies with relative displacement. Micro slip refers to a part of the hysteresis cycle between sticking and sliding in which the tangential force remains as a function of relative displacement. During micro slip, sliding takes place only between parts of the contact surfaces, while other parts do not undergo any relative motion. Gross slip refers to a part of the hysteresis cycle in which sliding takes place between all points the contact surfaces.

For the case of micro scale case, Mindlin [24] defined the ratio of the tangential stiffness to the normal stiffness between two bodies with same elastic constants by Eq. (17).

$$\frac{k_t}{k_n} = \frac{2(1-v)}{(2-v)}. \tag{17}$$

Filippi [25] then found that the Mindlin model correctly predicts the tangential stiffness under moderate normal load at frequencies 1–150 Hz in the state of micro slip. Then, tangential stiffness during gross slip did not show many differences to micro slip. Moreover, when the contact surfaces of structures are worn by rubbing under high loads in gross slip regime, the surfaces increase the contact stiffness. He then confirmed

that the tangential stiffness depends on the contact area and material properties, but independent of friction coefficient, relative velocity and excitation frequency.

In the case of contacted surface on a macro scale, Baltazar [26] defined the ratio between the tangential and the normal stiffness of mutually contacted two surfaces by

$$\frac{k_t}{k_n} = \frac{\xi}{\varphi}\frac{2(1-\nu)}{(2-\nu)}, \tag{18}$$

where the correction factor ξ/φ is determined by the effect of angular misalignment of contact. Using ultrasonic excitation on contact interface, Baltazar found that the correction factors ξ/φ for various roughness of surfaces should be almost within 0.63–0.69, and that the stiffness ratio k_t/k_n should be within 0.50–0.55. Nagy [27] found that aluminium material has its correction factor varying in 0.6–0.8, and that its stiffness ratio k_t/k_n is estimated between 0.48 and 0.64. In dynamic analysis, Sherif [28] made two model of steel cantilevers with tip masses whose flat ground were in contact under the effect of constant normal load. The flat contact surface of the tips was polished. He then excited the surface at frequency 10–400 Hz and obtained the ratio of dynamic tangential contact stiffness to tangential contact stiffness is around 0.25–0.35.

Based on the abovementioned investigation, we shall conclude that there is no unified model to obtain the value of the ratio between the tangential and the normal stiffness for macro scale and micro scale slip, because both scale slip models are formulated using many assumptions of the modelling about contact roughness in relative sliding conditions. There is no model that can clearly explain about tangential stiffness of sliding contact with respect to various conditions and parameters such as oscillation frequency, material, sliding speed, normal and tangential load. Nevertheless, in the case where contact interfaces are subjected to relative oscillatory motion due to vibration of structures at very low frequency, tangential stiffness during gross slip is not very different from that during micro slip.

In the next section, numerical simulations are presented about the normal and the tangential stiffness of different surface topographies whose characteristics and those of slider are listed in Table 1. Surface 1 is the roughest while surface 3 is the smoothest among the three surfaces. In the simulations, the ratio of the tangential contact stiffness to the normal one is assumed to be 0.2, and the apparent contact area is to be 10^{-4} m^2. Both stiffnesses as a function of normal force are shown in Fig. 3. It is found in Fig. 3 that smoother the surface and higher the normal load will have higher values of the normal and the tangential contact stiffness.

2.3. Friction coefficient

Physicists and engineering researchers have set up several theories about friction coefficient confirmed by experimental studies from the viewpoints of nano-scale and macro-scale. However, a unified friction theory over all the scales is still missing. Friction force in an interface depends on many variables such as material properties, geometry, and atmospheric properties. The mechanism of friction force is described by two kinds of components. One is the mechanical component related to the deformation of asperities, fracture and shear of contaminant, and lubricant films. Another one is the chemical component directly related to atomic and

Table 1
Some surface topography

Parameter	Surface 1	Surface 2	Surface 3	Slider
Max radius, R_p (μm)	1.6	0.80	0.2	0.2
Mean spacing, S_m (μm)	150	80	50	50
Standard deviation, σ (μm)	0.75	0.35	0.1	0.1
Asperity density, η (cm^{-2})	5000	15000	36000	36000
Modulus elasticity, E (Nm^{-2})	2.11×10^{11}	2.11×10^{11}	2.11×10^{11}	2.11×10^{11}
Poisson's ratio, ν	0.3	0.3	0.3	0.3

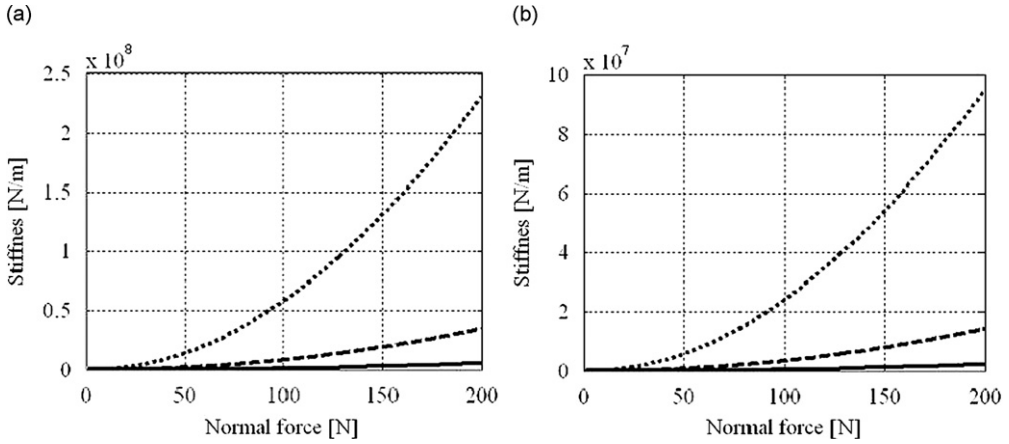

Fig. 3. Contact stiffness in three surfaces whose topography characteristics described in Table 1: (a) normal contact stiffness; (b) tangential contact stiffness. ..... surface contact 1, – – –– surface contact 2, ····· surface contact 3.

molecular interaction of the mating surface (adhesion). There is no simple correlation between friction coefficient and these factors of mechanical and chemical components [29].

In the case of sliding rough surfaces with metallic interface, the mechanical component will be the most important contributor to the resultant friction force. The contribution to friction force will be generated by the mechanical resistance due to elastic and plastic deformation of the asperities and the adhesive force between the mutually contacted asperities.

Generally, the coefficient of dry friction μ can be expressed as the sum of adhesion component μ_a, deformation (plowing) component μ_d, and ratchet component μ_r. The deformation component, in the presence of wear or contamination particles, is the sum of asperity summit deformation component μ_{ds} and particle deformation component μ_{dp} [30]. In short, the total coefficient of friction is expressed by

$$\mu = \mu_a + \mu_{ds} + \mu_{dp} + \mu_r. \tag{19}$$

An experimental investigation [31] showed that the correlation between friction and adhesion depends on many parameters such as temperature, sliding velocity, load, and relative humidity in a great complexity, therefore the correlation is difficult to be modelled.

For instance, Eriksson et al. [32] investigated the dependence of the friction coefficient regarding brake pads of automobiles upon various pressure, speed, and roughness of the sliding surface. They concluded that it was very hard to establish an accurate model of the friction in brake systems because of its extreme complexity even to cover only the most important phenomenon. They found experimentally that the coefficient of friction of pad varies between 0.3 and 0.6.

3. A two-degree of freedom model

Numerical simulations are carried out in this section to investigate the essential properties of mode coupling instability using a single particle mass model having two degrees of freedom as shown in Fig. 4. This model is developed using the minimal model of the mode coupling analysis by Hoffman [19]. It takes the effect of tangential contact stiffness to the mechanism of generating squeal noise into account.

The particle mass m is supported by two linear springs, whose stiffness coefficients are denoted by k_1 and k_2, and two viscous dampers whose coefficients are expressed as c_1 and c_2 on a moving horizontal plane. The stroke line of the spring k_2 and the damper c_2 lean toward from the normal direction. The contact stiffness between the mass and the moving plane is modelled using a spring k_n for the normal component and another spring k_t for the tangential component. The mass is contacting to the moving plane at a constant velocity. Point O denotes the contact point. F_n and F_f represent the normal force and the friction force that are working at the point as depicted in Fig. 4.

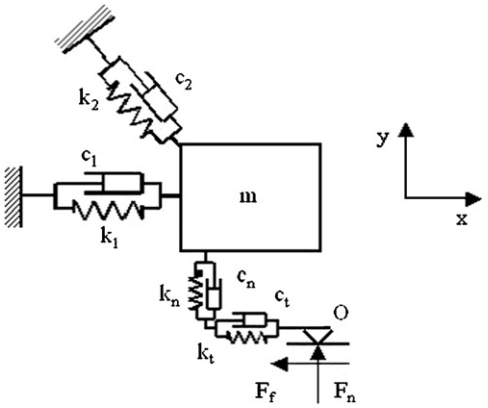

Fig. 4. Two-degree of freedom model.

Under the assumption that the relative displacement of point O to the mass m can be negligible, the equations of motion of the mass can be formulated as follows:

$$m\ddot{x} + c_1\dot{x} + \frac{\sqrt{2}}{2}c_2\dot{x} + c_t\dot{x} - \frac{\sqrt{2}}{2}c_2\dot{y} + k_1x + \frac{\sqrt{2}}{2}k_2x + k_tx - \frac{\sqrt{2}}{2}k_2y = -F_f,$$
$$m\ddot{y} - \frac{\sqrt{2}}{2}c_2\dot{x} + \frac{\sqrt{2}}{2}c_2\dot{y} + c_n\dot{y} - \frac{\sqrt{2}}{2}k_2x + \frac{\sqrt{2}}{2}k_2y + k_ny = F_n. \tag{20}$$

If the friction force can be approximated by $F_f = \mu k_n y$ and damping coefficients are to be all zeros, the equations of the autonomous system can be written by Eq. (21) in the matrix form.

$$\begin{bmatrix} m & 0 \\ 0 & m \end{bmatrix}\begin{Bmatrix} \ddot{x} \\ \ddot{y} \end{Bmatrix} + \begin{bmatrix} k_1 + \frac{\sqrt{2}}{2}k_2 + k_t & -\frac{\sqrt{2}}{2}k_2 + \mu k_n \\ -\frac{\sqrt{2}}{2}k_2 & \frac{\sqrt{2}}{2}k_2 + k_n \end{bmatrix}\begin{Bmatrix} x \\ y \end{Bmatrix} = \begin{Bmatrix} 0 \\ 0 \end{Bmatrix}. \tag{21}$$

Since the stiffness matrix in Eq. (21) is nonsymmetric, it is mathematically obvious that this system has complex eigenvalues when it has certain values for its components. Setting $m = 1\,\text{kg}$, $k_1 = 10^8\,\text{N/m}$ and $k_2 = 5 \times 10^7\,\text{N/m}$, numerical simulations are carried out using the model in order to investigate the effect of the normal contact stiffness, the tangential contact stiffness and the friction coefficient to the occurrence of the coupled-mode instability. Note that the normal contact stiffness, the tangential contact stiffness and the friction coefficient actually correlate to surface topography and that the damping of the system is neglected.

Fig. 5 shows the frequency response functions (FRFs) of the mass in various normal and tangential contact stiffness due to friction force under the assumption of linear contact stiffness. The friction coefficient is kept a constant value of 0.5, and the ratio of the tangential contact stiffness to the normal one is set to be 0.2. It is clearly found that there are two peaks of natural modes in the 3D graphs of FRFs, and then they are coming closer and closer with the increase of contact stiffness. The couple of modes then merge from a point at a certain value of contact stiffness, and afterwards, separate again. In Fig. 5, although the peak levels of FRFs at the merged natural frequencies are plotted lower than the original levels of two peaks in the un-merged condition, the responses rise exponentially time because of the positive growth rate of the response.

The response of the modal system is generally expressed by $q_i(t) = Q_i e^{(a+jb)t}$, where the imaginary part of the exponential power represents a natural frequency and the real part represents the growth rate of the response. The natural frequency, growth rate of the model at various values of contact stiffness and friction coefficients are presented in Fig. 6.

There are two layers of natural frequency graphics basically in Fig. 6. The lower and the upper layer correspond to the first and the second natural frequency, respectively. The equal and relatively flat regions of the layers represent that both natural frequencies are being merged and the growth rates are positive in the

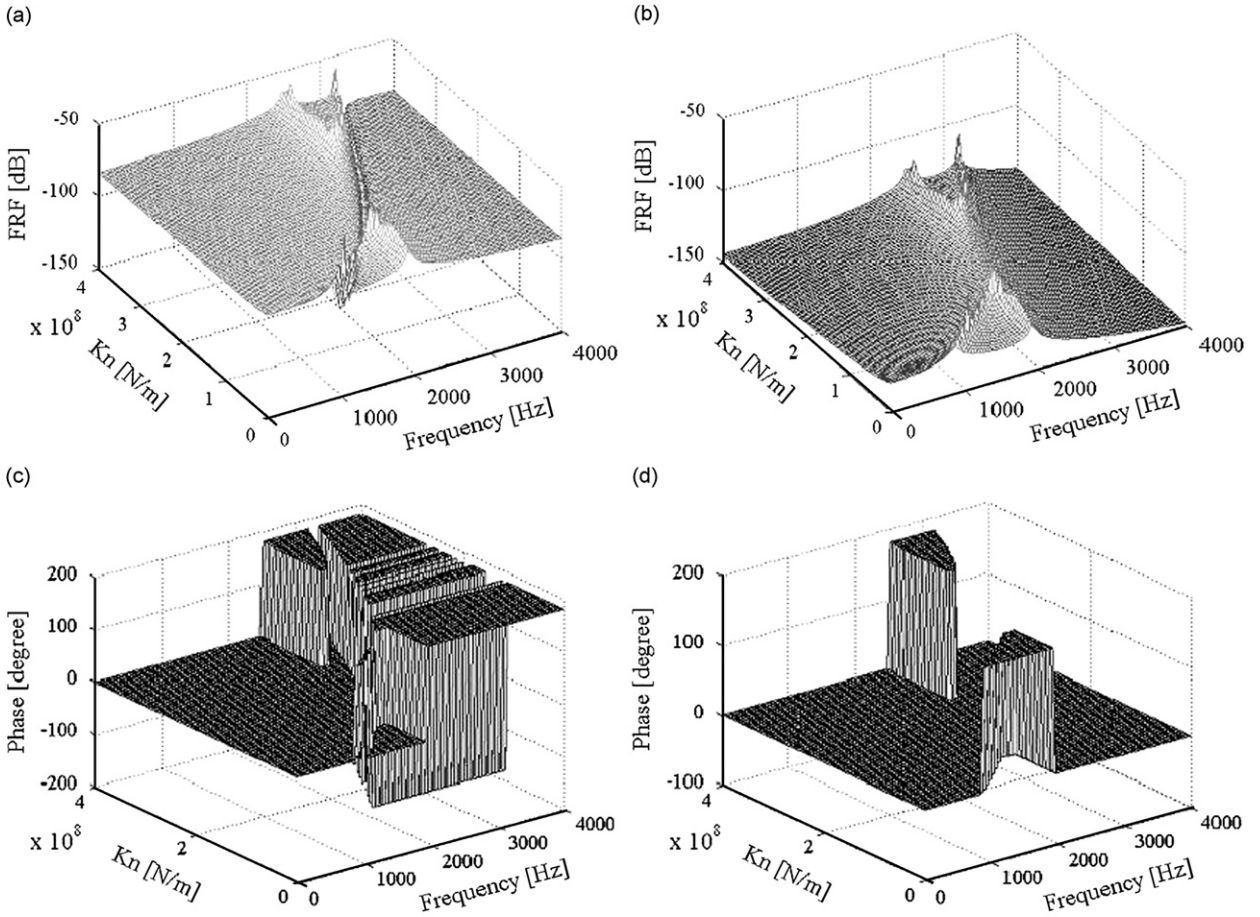

Fig. 5. FRF and its phase mapping with respect to changing normal contact stiffness: (a) FRF of horizontal response; (b) FRF of vertical response; (c) phase of horizontal response; and (d) phase of vertical direction.

regions. It means that the vibration response at this merged natural frequency increases exponentially in the time. In other words, this merged frequency is unstable.

Here, let us terminologically define "critical friction coefficient" to describe the lowest friction coefficient that can make the system unstable. Critical friction coefficients form as an almost parabolic function of normal contact stiffness as shown in Fig. 6. Fig. 6(a) shows the result in the case where the tangential contact stiffness is set to be zero. There are two regions of the normal contact stiffness in which no unstable vibration occurs with any value of the friction coefficient when the tangential contact stiffness is zero. In addition, even in the unstable region, there are some points at which the response of the system is stable Therefore, it is difficult to predict which kind of response occurs, unstable or stable. In the region of very lower friction coefficient, the merging of two natural frequencies does not occur in all the region of normal contact stiffness although the two natural frequencies gradually approach each other and separate away as the contact stiffness increases. In this condition, the model has separated natural frequencies with positive real eigenvalues and stable response.

Fig. 6(b) shows the result in the case where the tangential contact stiffness is set 0.2 times of the value of the normal one. There is only one region of the normal contact stiffness in which no unstable vibration occurs with any value of the friction coefficient. The region is placed at the narrow range of the normal contact stiffness from zero. It is found with the result that the unstable region is also affected by the tangential contact stiffness. The effect of the tangential contact stiffness can be observed as the difference between Fig. 6(a) and (b). A higher value ($\alpha > 0$) of the tangential contact stiffness will change and make the possibility of the system

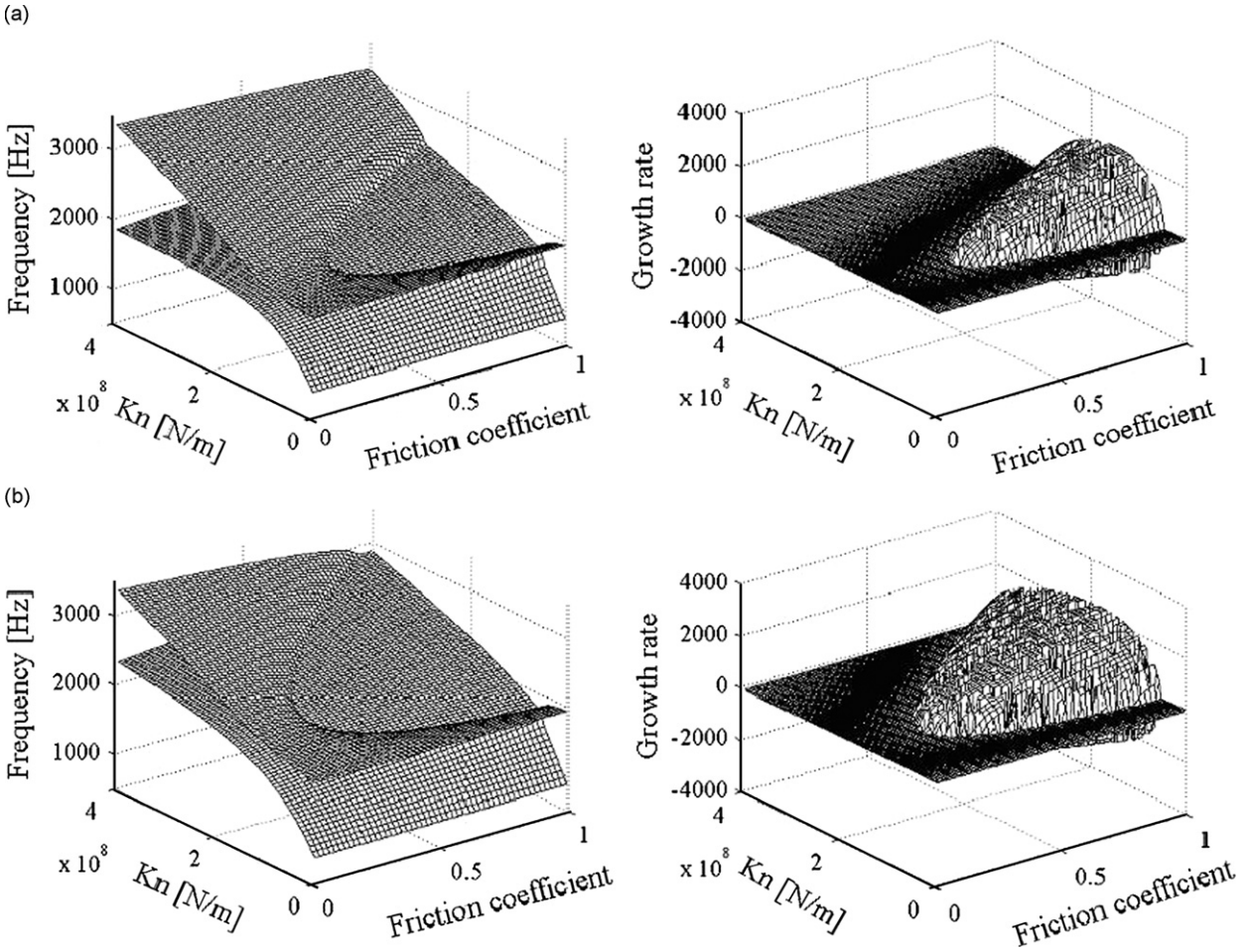

Fig. 6. Natural frequency and growth rate mapping about two-degree of freedom model: (a) $\alpha = k_t/k_n = 0$; (b) $\alpha = k_t/k_n = 0.2$.

instability higher within certain values of the normal contact stiffness, and will decrease the critical friction coefficient more.

It is well known that changing the dynamic characteristics of structures will change the unstable region of responses. Structures have their own unstable regions depending on their contact parameters. Consequently, a structure will generate squeal noise at one of particular frequencies that can make it possible to generate squeal noise under certain contact parameters and topography conditions. Then, it is difficult to predict the occurrence of squeal noise and its frequency. A smooth surface with high normal contact stiffness in sliding contact interface tends to generate squeal noise at relatively high frequencies. On the other hand, rough surface with low normal contact stiffness tends to generate squeal noise at relatively low frequencies.

4. A multi-degrees of freedom model

The second numerical investigation is conducted using a simple space frame model with a friction contact at one edge shown in Fig. 7. The area of the frame cross section is set to be a constant over the whole frame. Using the finite element method, the frame is made with eight finite elements, and the friction force is assumed to be applied only in x-direction of global coordinate system. The value of the normal contact stiffness K_x is set variously within $1.10^8 - 4.10^8$, and the ratio of the tangential contact stiffness to the normal one is set to be 0.2 ($K_y = K_z = K_{mx} = 0.2K_x$).

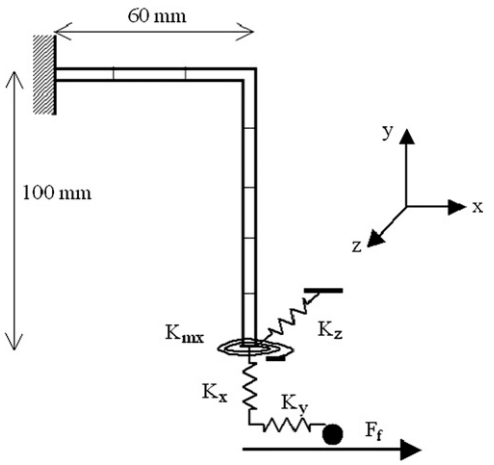

Fig. 7. Space frame as a case study, $A = 9.6 \times 10^{-5}\,\mathrm{m}^2$, $\rho = 7850\,\mathrm{kg/m}^3$, $E = 2.1 \times 10^{11}\,\mathrm{N/m}$, $E = 8.0 \times 10^{9}\,\mathrm{N/m}$, local inertia $I_x = 8.2 \times 10^{-9}\,\mathrm{m}^{-4}$, $I_y = 8.192 \times 10^{-9}\,\mathrm{m}^{-4}$, $I_z = 7.2 \times 10^{-11}\,\mathrm{m}^{-4}$.

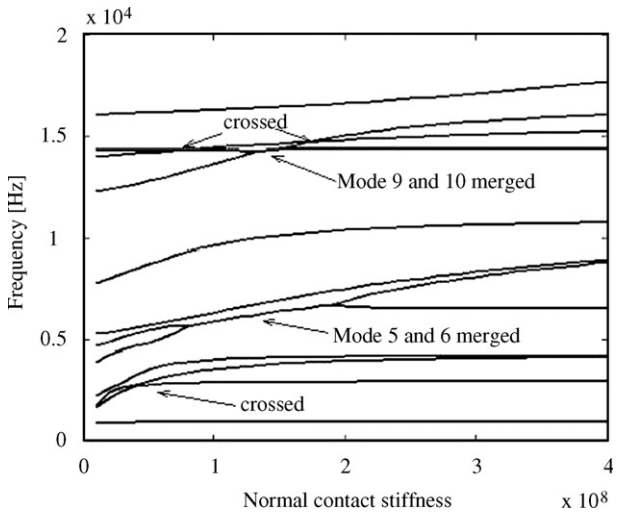

Fig. 8. The change of natural frequencies with respect to normal contact stiffness.

Under the condition of setting the friction coefficient at 0.5 of the constant value, some natural frequencies from the first order change depending on the values of the normal contact stiffness as shown in Fig. 8. Increasing the normal contact stiffness caused by the change of the surface topography makes some natural frequency approach closer to adjacent one each other, but all of them do not merge. Only a few natural frequencies among them merge and the others just cross each other. To reveal the mechanism of making such crossing and merging of natural frequencies is still on a half way of investigation and out of the scope of this paper.

The focus of this discussion is to investigate the correlation between merging natural frequencies and contact stiffness by means of numerical simulation. Keeping the friction coefficient at 0.5 of the constant value, and the normal contact stiffness within $0.9 \times 10^8 - 1.9 \times 10^8\,\mathrm{N/m}$, the 5th and the 6th natural mode are merged mutually and the eigenvalue of the resultant merging natural mode becomes a complex number with a positive real part. In another very limited range around $1.3 \times 10^8 - 1.5 \times 10^8\,\mathrm{N/m}$ of the contact stiffness, the 9th and the 10th mode are merged. These merging imply that squeal may coincide at two frequencies on the condition that the topography condition and the normal pressure of the contact make the normal contact

stiffness around $1.3 \times 10^8 - 1.5 \times 10^8$ N/m and the friction coefficient at 0.5. If the normal contact stiffness is set to be a value between $0.9 \times 10^8 - 1.9 \times 10^8$ N/m except for the range of $1.3 \times 10^8 - 1.5 \times 10^8$ N/m, the friction will generate squeal noise at only single frequency, and no squeal noise is generated out of the range of normal contact stiffness.

Fig. 9 shows the growth rates of the eigenvalues from the 1st to the 12th order with respect to various values of friction coefficient and normal contact stiffness. As already mentioned above, only two pairs of natural

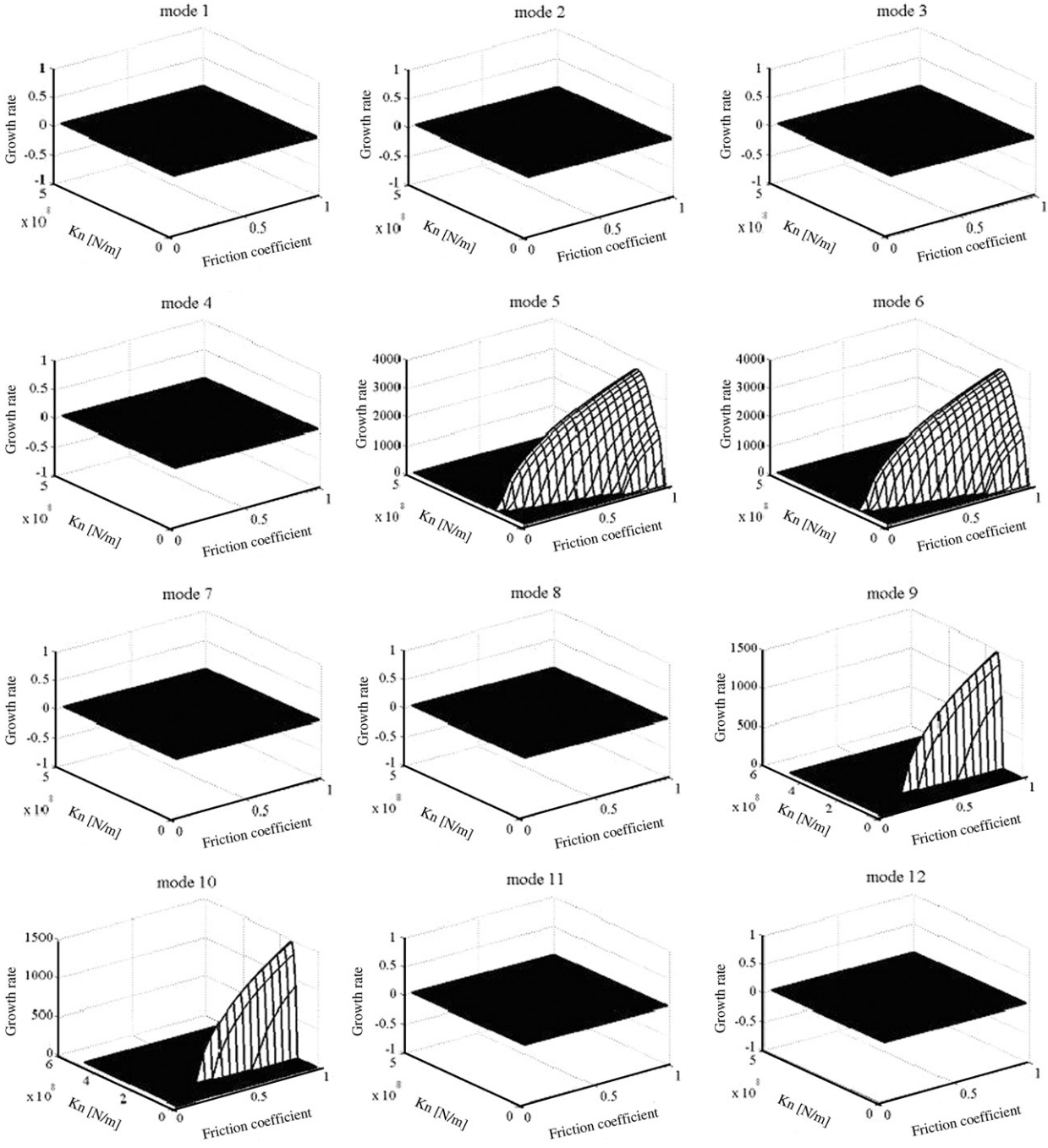

Fig. 9. Growth rates of the first to the 12 natural frequencies.

modes tend to merge. Namely, they are the pair of the 5th and the 6th mode and the pair of the 9th and the 10th mode. The pair of the 5th and the 6th mode has higher possibility to merge and generate squeal noise than the pair of the 9th and the 10th. The pair of the 9th and the 10th order will generate squeal noise in relatively high friction coefficients and a very limited range of normal contact stiffness. Note here that it is not understood well yet what parameters of the contact condition make natural modes merge and/or cross in general.

The abovementioned mechanism in this section will be able to explain some cases of the relation between squeal noise and surface roughness described in the first section of "Introduction". A structure will generate squeal noise on the condition of only a certain contact parameter and a different contact surface topography. A very stiff structure having its natural frequencies at high frequencies will grow high possibility to generate squeal noise due to its high normal contact stiffness and smooth surface. This will be able to explain why disc brakes tend to produce squeal noise in relatively smooth surface or small plateaus condition [11] and why the experiment reported in Ref. [17] generate squeal noise in rougher surface condition. Squeal noise at different frequency may be generated in different contact parameter conditions as reported by Chen [13]. Of course, more detailed investigation is needed to explain the phenomena in each case.

5. Conclusions

It has been shown in this paper that the contact parameters; i.e. normal and tangential contact stiffness about the sliding contact surface, and the friction coefficient play a significant role to generate unstable mode coupling in a structure with friction. Unstable mode coupling occurs when the dynamic parameters of a structure and the contact parameters make the stiffness matrix asymmetric. Therefore, since a few pairs of adjacent eigenvalues and eigenvectors merge, unstable vibration to generate squeal noise will be generated. This unstable mode coupling occurs at certain range of the values of contact stiffness and friction coefficient. Higher friction coefficient will raise the possibility of generating mode coupling in a structure. To reveal the mechanism of merging eigenvalues is still on a half way of investigation from the viewpoints of mechanics based on mathematics.

In the case of friction in rough surface of sliding contact interface, the contact parameters depend on the topography characteristics of contact surface as long as the load applied at the interface is not so big to destroy all asperities. The contact of rougher surface has lower contact stiffness than of smoother one. Because of the interaction between the dynamic parameters of structure and the contact parameters to form mode coupling, it can be understood why a structure generate squeal noise in relative rough surface of sliding contact interface and why others generate in smoother surface. A very stiff structure having its natural frequencies at high frequencies will generate squeal noise in relative smooth surface and vice versa.

Since the relation between contact parameters and the parameters of surface topography is very complex and cannot be explained in a simple formula, it is not easy to judge whether a structure will generate squeal noise or not at a value of the roughness of sliding contact surface. However, the mechanism explained in this paper can describe the phenomena of generating squeal noise corresponding to the surface topography.

The next research works should be focused at least on following two aspects for finding a better analysis of squeal noise using mode-coupling model. The first is the aspect of experimental investigation to conform such theoretical phenomena discussed in this paper, and the second aspect is of analysis of system's nonlinearity caused by nonlinear contact stiffness.

References

[1] M.J. Rudd, Wheel/rail noise–part II: wheel squeal, *Journal of Sound and Vibration* 46 (1976) 381–394.
[2] C.J.M. Van Ruiten, Mechanism of squeal noise generated by trams, *Journal of Sound and Vibration* 120 (1988) 245–253.
[3] M.A. Heckl, I.I. Abrahams, Curve squeal of train wheels, part I: mathematical model for its generations, *Journal of Sound and Vibration* 229 (2000) 669–693.
[4] M.A. Heckl, Curve squeal of train wheels, part 2: which wheel modes are prone to squeal, *Journal of Sound and Vibration* 229 (2000) 695–707.
[5] F.G. de Beer, M.H.A. Janssens, P.P. Kooijman, Squeal noise of rail-bound vehicles influenced by lateral contact position, *Journal of Sound and Vibration* 267 (2003) 497–507.

[6] O. Ouyang, J.E. Mottershead, Friction-induced parametric resonance in discs: effect of a negative friction–velocity relationship, *Journal of Sound and Vibration* 209 (1998) 251–264.
[7] T. Jearsiripongkul, D. Hochlenert, U. Von Wagner, P. Hagerdorn, A nonlinear floating calliper disk brake model to incorporate squeal, *SAE International*, 2004, 2004-01-2802.
[8] O. Ouyang, J.E. Mottershead, W. Li, A moving-load model for disc brake stability analysis, *Transactions of ASME Journal of Vibration and Acoustics* 125 (2003) 53–58.
[9] C. Hung, J. Chung, M. Donley, Mode coupling phenomenon of brake squeal dynamics, *SAE International*, 2003, 2003-01-1624.
[10] M. Eriksson, F. Bergman, S. Jacobson, Surface characterization of brake pads after running under silent and squealing condition, *Wear* 232 (1999) 163–167.
[11] F. Bergman, M. Eriksson, S. Jacobson, Influence of disc topography on the generation of brake squeal, *Wear* 225–229 (1999) 621–628.
[12] R.A. Ibrahim, Friction-induced vibration, chatter, squeal, and chaos—part II: dynamics and modeling, *ASME Applied Mechanic Review* 47 (1994) 227–253.
[13] G.X. Chen, Z.R. Zhou, Experimental observation of the initiation process of friction-induced vibration under reciprocating sliding condition, *Wear* 259 (2005) 277–281.
[14] G.X. Chen, Z.R. Zhou, P. Kapsa, L. Vincent, Experimental investigation into squeal under reciprocating sliding, *Tribology International* 36 (2003) 961–971.
[15] N. Hoffman, L. Gaul, Effect of damping on mode-coupling instability in friction induced oscillations, *ZAMM Zeitschrift fur Angewante Mathematik und Mechanik* 83 (8) (2003) 524–534.
[16] D.T. Eady, J. Kalousek, C.C. Chiddick, The role of high positive friction (HPF) modifier in the control of short pitch corrugations and related phenomena, *Wear* 253 (2002) 185–192.
[17] G.X. Chen, Z.R. Zhou, P. Kapsa, L. Vincent, Effect of surface topography on formation squeal under reciprocating sliding, *Wear* 253 (2002) 411–423.
[18] H.A. Sherif, Investigation on effect of surface topography of pad/disc assembly on squeal generation, *Wear* 257 (2004) 687–695.
[19] N. Hoffman, M. Fischer, R. Allgaier, L. Gaul, A minimal model for studying properties of the mode-coupling type instability in friction induced oscillation, *Mechanics Research Communication* 29 (2002) 197–205.
[20] J.A. Greenwood, J.P.B. Williamson, Contact of nominally flat surfaces, *Proceedings of the Royal Society of London A* 316 (1970) 97–121.
[21] J.A. Greenwood, J.H. Tripp, The elastic contact of rough spheres, *Journal of Applied Mechanics* (1967) 153–159.
[22] N. Tayebi, A.A. Polycarpou, Modeling the effect of skewness and kurtosis on the static friction coefficient of rough surfaces, *Tribology International* 37 (2004) 491–505.
[23] B. Bhushan, Contact mechanics of rough surfaces in tribology: multiple asperity contact, *Tribology Letter* 4 (1998) 1–35.
[24] R.D. Midlin, Compliance of elastic bodies in contact, *Transactions of the ASME Journal of Applied Mechanics* 16 (1949) 259–268.
[25] S. Filippi, Experimental validation of contact models for small tangential displacement, *XXXII Covegno Nazionale dell'Associazone Italianz per l'Analisi delle sollecitazioni*, *AIAS*, 2003, paper 112.
[26] A. Baltazar, S.I. Rockhlin, C. Pecorari, On the relationship between ultrasonic and micro mechanical properties of contacting rough surfaces, *Journal of the Mechanics and Physics of Solids* 50 (2002) 1397–1416.
[27] P.B. Nagy, Ultrasonic classification of imperfect interfaces, *Journal of Nondestructive Evaluation* 11 (1992) 127–139.
[28] H.A. Sherif, Mode of zero wear in mechanical systems with dry contact, *Tribology International* 38 (2005) 59–68.
[29] M.T. Bengisu, A. Akay, Relation of dry friction to surface roughness, *Transaction of the ASME Journal of Tribology* 119 (1997) 18–24.
[30] M. Nosonovsky, B. Bhusan, Scale effect in dry friction during multiple asperity contact, *Transactions of the ASME Journal of Tribology* 127 (2006) 37–46.
[31] H. Yoshizawa, Y.L. Chen, J. Israelachvili, Fundamental mechanism of interfacial friction, 1. Relation between adhesion and friction, *Journal of Physical Chemistry* 97 (1993) 4128–4140.
[32] M. Eriksson, F. Bergman, S. Jacobson, On the nature of tribological contact in automotives brake, *Wear* 252 (2002) 26–36.